J Bioenerg Biomembr (2013) 45:189–202
DOI 10.1007/s10863-012-9483-7

Dynamic buffering of mitochondrial Ca^{2+} during Ca^{2+} uptake and Na^{+}-induced Ca^{2+} release

Christoph A. Blomeyer · Jason N. Bazil · David F. Stowe · Ranjan K. Pradhan · Ranjan K. Dash · Amadou K. S. Camara

Received: 10 July 2012 / Accepted: 8 October 2012 / Published online: 7 December 2012

Abstract In cardiac mitochondria, matrix free Ca^{2+} ($[Ca^{2+}]_m$) is primarily regulated by Ca^{2+} uptake and release via the Ca^{2+} uniporter (CU) and Na^{+}/Ca^{2+} exchanger (NCE) as well as by Ca^{2+} buffering. Although experimental and computational studies on the CU and NCE dynamics exist, it is not well understood how matrix Ca^{2+} buffering affects these dynamics under various Ca^{2+} uptake and release conditions, and whether this influences the stoichiometry of the NCE. To elucidate the role of matrix Ca^{2+} buffering on the uptake and release of Ca^{2+}, we monitored Ca^{2+} dynamics in isolated mitochondria by measuring both the extra-matrix free $[Ca^{2+}]$ ($[Ca^{2+}]_e$) and $[Ca^{2+}]_m$. A detailed protocol was developed and freshly isolated mitochondria from guinea pig hearts were exposed to five different $[CaCl_2]$ followed by ruthenium red and six different [NaCl]. By using the fluorescent probe indo-1, $[Ca^{2+}]_e$ and $[Ca^{2+}]_m$ were spectrofluorometrically quantified, and the stoichiometry of the NCE was determined. In addition, we measured NADH, membrane potential, matrix volume and matrix pH to monitor Ca^{2+}-induced changes in mitochondrial bioenergetics. Our $[Ca^{2+}]_e$ and $[Ca^{2+}]_m$ measurements demonstrate that Ca^{2+} uptake and release do not show reciprocal Ca^{2+} dynamics in the extra-matrix and matrix compartments. This salient finding is likely caused by a dynamic Ca^{2+} buffering system in the matrix compartment. The Na^{+}- induced Ca^{2+} release demonstrates an electrogenic exchange via the NCE by excluding an electroneutral exchange. Mitochondrial bioenergetics were only transiently affected by Ca^{2+} uptake in the presence of large amounts of $CaCl_2$, but not by Na^{+}- induced Ca^{2+} release.

Keywords Mitochondria · Ca^{2+} uniporter · Na^{+}/Ca^{2+} exchanger · Ca^{2+} buffering · Bioenergetics

Introduction

Homeostasis of mitochondrial Ca^{2+} is well maintained by a balance of Ca^{2+} uptake, sequestration and release mechanisms (Santo-Domingo and Demaurex 2010; Gunter and Sheu 2009; Griffiths 2009). The main route for Ca^{2+} uptake is the ruthenium red-sensitive Ca^{2+} uniporter (CU) (Gunter and Pfeiffer 1990; Graier et al. 2007), which is in large part driven by the negative mitochondrial membrane potential ($\Delta\Psi_m$) and the Ca^{2+} gradient across the inner mitochondrial membrane (IMM) (Gunter and Sheu 2009; Saotome et al. 2005; Dash et al. 2009; Dedkova and Blatter 2008). The negative $\Delta\Psi_m$ is generated by H^{+} pumping in the respiratory chain, which also creates a H^{+} gradient across the IMM resulting in an alkaline matrix pH (pH_m). The ability of the matrix compartment to sequester large amounts of Ca^{2+} is attributed to its Ca^{2+} loading capacity with a strong buffering power (Olson et al. 2012). It is widely assumed that the formation of Ca^{2+}-phosphate precipitates inside the alkaline matrix plays an important role in the sequestration of large quantities of Ca^{2+} (Starkov 2010; Chalmers and Nicholls

Electronic supplementary material The online version of this article (doi:10.1007/s10863-012-9483-7) contains supplementary material, which is available to authorized users.

C. A. Blomeyer · D. F. Stowe · A. K. S. Camara (✉)
Department of Anesthesiology, Medical College of Wisconsin,
8701 Watertown Plank Road,
Milwaukee, WI 53226, USA
e-mail: aksc@mcw.edu

J. N. Bazil · R. K. Pradhan · R. K. Dash
Biotechnology and Bioengineering Center
and Department of Physiology, Medical College of Wisconsin,
8701 Watertown Plank Road,
Milwaukee, WI 53226, USA

D. F. Stowe
Research Service, Zablocki Veterans Affairs Medical Center,
5000 W. National Avenue,
Milwaukee, WI 53295, USA

2003; Chinopoulos and Adam-Vizi 2010). Under pathologic conditions (e.g. during ischemia and reperfusion), a rapid and massive uptake of Ca^{2+} can overwhelm the matrix Ca^{2+} buffering system. By exceeding a certain threshold of mitochondrial Ca^{2+} the mitochondrial permeability transition pore (mPTP) opens and releases pro-apoptotic proteins, and an enormous amount of Ca^{2+} into the cytosol, resulting in mitochondrial damage and cell death (Brookes et al. 2004; Halestrap 2009; Bernardi and Rasola 2007; Camara et al. 2010). The main route for release of mitochondrial Ca^{2+} in excitable tissues (e.g. brain, heart) is the mitochondrial Na^+/Ca^{2+} exchanger (NCE) (Gunter and Pfeiffer 1990; Dedkova and Blatter 2008; Hoppe 2010), which in its forward mode extrudes Ca^{2+} in exchange for cytosolic Na^+ (Pradhan et al. 2010a). In addition to Ca^{2+} transport via the CU and NCE, mitochondrial Ca^{2+} homeostasis in energized mitochondria may also be modulated by the $\Delta\Psi_m$, ΔpH, Ca^{2+}/H^+ exchanger (CHE) and Na^+/H^+ exchanger (NHE).

It is noteworthy that the proteins forming the CU and NCE have been recently identified (Palty et al. 2010; Baughman et al. 2011; De Stefani et al. 2011). However, the precise stoichiometry of Na^+/Ca^{2+} exchange via the NCE remains unsettled. On the one hand, some experimental studies indicate a $2Na^+$:$1Ca^{2+}$ (electroneutral) exchange (Brand 1985; Paucek and Jaburek 2004). On the other hand, other experimental studies indicate a $3Na^+$:$1Ca^{2+}$ (electrogenic) exchange (Baysal et al. 1994; Jung et al. 1995; Crompton et al. 1976). An electrogenic exchange would be regulated by the $\Delta\Psi_m$ (Jung et al. 1995), since additional positive charges would move into the matrix during the forward mode of the NCE (Crompton et al. 1976; Kim and Matsuoka 2008). Furthermore, biophysical computational approaches have been used to characterize the kinetics and stoichiometry of the NCE (Pradhan et al. 2010a; Dash and Beard 2008). In these computational studies, published data from previous experimental studies (Paucek and Jaburek 2004; Kim and Matsuoka 2008; Cox and Matlib 1993) on the NCE kinetics were utilized to predict the impact of extra-matrix $[Ca^{2+}]$, $[Na^+]$ and $\Delta\Psi_m$ on the NCE function. However, those approaches did not unambiguously identify the actual stoichiometry of the NCE (Pradhan et al. 2010a) due to limited available experimental data.

Previous experiments on Ca^{2+} regulation in heart mitochondria have provided insights into the CU and NCE dynamics by investigating the effects of adding either one single bolus of $CaCl_2$ and multiple boluses of NaCl, or multiple boluses of $CaCl_2$ and one single bolus of NaCl to the extra-matrix compartment (Jung et al. 1995; Crompton et al. 1976; Kim and Matsuoka 2008; Cox and Matlib 1993; Wei et al. 2011). Furthermore, these studies measured changes only in either extra-matrix free $[Ca^{2+}]$ ($[Ca^{2+}]_e$) or matrix free $[Ca^{2+}]$ ($[Ca^{2+}]_m$). Recently, a study on mitochondrial Ca^{2+} uptake using repeated boluses of Ca^{2+} simultaneously measured changes in $[Ca^{2+}]_e$ and $[Ca^{2+}]_m$ (Wei et al. 2012). However, to date it has not been well elucidated how matrix Ca^{2+} buffering influences Ca^{2+} uptake via the CU under multiple Ca^{2+} loading conditions and how buffering affects Ca^{2+} release via the NCE by different Na^+ perturbations.

In the present study, our aim was to examine the CU and NCE dynamics in isolated cardiac mitochondria under various Ca^{2+} uptake and release conditions by monitoring the effects of different amounts of $CaCl_2$ and NaCl added to the extra-matrix compartment on changing both the $[Ca^{2+}]_e$ and $[Ca^{2+}]_m$. We postulated that Ca^{2+}- and Na^+-induced changes in $[Ca^{2+}]_e$ and $[Ca^{2+}]_m$ exhibit dissimilar dynamics that are due to a strong and dynamic Ca^{2+} buffering of the matrix compared to the extra-matrix compartment. To test this, we used established techniques to isolate mitochondria from guinea pig hearts and to measure $[Ca^{2+}]_e$ and $[Ca^{2+}]_m$ (Haumann et al. 2010; Heinen et al. 2007). A detailed protocol was developed to focus on the dynamics of Ca^{2+} transport via the CU and NCE. To better understand the dynamic modulation of mitochondrial Ca^{2+} homeostasis and its impact on mitochondrial bioenergetics, additional experiments were conducted to monitor changes in NADH (redox state), $\Delta\Psi_m$, pH_m, and matrix volume.

Our data on $[Ca^{2+}]_e$ and $[Ca^{2+}]_m$ during Ca^{2+} uptake and Na^+-induced Ca^{2+} release were then utilized to quantify the mitochondrial Ca^{2+} buffering system using a mathematical model (see our companion paper (Bazil et al. 2012)). Indeed, findings derived from this computational study (Bazil et al. 2012) corroborate our experimental observations regarding the existence of a dynamic matrix Ca^{2+} buffering system during variations in Ca^{2+} uptake and release.

Methods

Mitochondrial isolation

All experiments conformed to the Guide for the Care and Use of Laboratory Animals and were approved by the Medical College of Wisconsin Institutional Animal Care and Use Committee (IACUC). Mitochondria from guinea pig hearts were isolated as previously described (Haumann et al. 2010; Heinen et al. 2007). Guinea pigs (250–350 g) were anesthetized by intraperitoneal injection of 30 mg ketamine, and 700 units of heparin for anticoagulation. Hearts (n=64) were excised and minced to approximately 1 mm^3 pieces in ice-cold isolation buffer containing 200 mM mannitol, 50 mM sucrose, 5 mM KH_2PO_4, 5 mM 3-(N-morpholino) propanesulfonic acid (MOPS), 1 mM EGTA and 0.1 % bovine serum albumin (BSA). Buffer pH was adjusted with KOH to 7.15. The minced pieces were suspended in 2.65 ml ice-cold buffer with 5U/ml protease (from *Bacillus licheniformis*), and homogenized at low speed for 30 s. Afterwards, 17 ml ice-cold isolation buffer was added and the

suspension was again homogenized for 30 s and centrifuged at 8,000*g* for 10 min. The supernatant was discarded and the pellet was re-suspended in 25 ml ice-cold isolation buffer and centrifuged at 900*g* for 10 min. The supernatant was recovered and centrifuged once more at 8,000*g* to yield the final mitochondrial pellet, which was re-suspended in isolation buffer and kept on ice (4 °C). The mitochondrial protein concentration was measured using the Bradford method (Bradford 1976) and diluted with isolation buffer to a defined protein concentration of 5 mg/ml and incubated with the appropriate dye or the vehicle (DMSO). Incubated mitochondria were re-suspended in 25 ml ice-cold isolation buffer and re-centrifuged at 8,000*g*. Subsequently, the dye-loaded pellet was re-suspended in cold isolation buffer, and the protein concentration was measured again, using the Bradford method (Bradford 1976), and diluted to 12.5 mg/ml. The final mitochondrial suspension was stored in packed ice (4 °C) and all subsequent experiments were conducted within 6 h after the last step of the isolation procedure.

Experimental groups and protocols

Isolated mitochondria were exposed to five different amounts of $CaCl_2$ and to six different amounts of NaCl resulting in 30 groups overall. For measurements of $[Ca^{2+}]_m$ or $[Ca^{2+}]_e$, isolated mitochondria of each preparation were randomly assigned to two different $CaCl_2$ groups and their six NaCl subgroups. Corresponding NADH measurements were conducted from the same mitochondrial preparation. Since the combinations of different $[CaCl_2]$ and [NaCl] for measurements of $\Delta\Psi_m$, pH_m and matrix volume were reduced to nine groups, all groups were tested from the same mitochondrial preparation for that specific day. Experiments were always repeated (n=3–4) with mitochondria obtained from different hearts. Experimental buffer, which was adjusted with KOH to pH 7.15, contained 130 mM KCl, 5 mM K_2HPO_4, 20 mM MOPS and 0.1 % BSA. Since the mitochondria were suspended in isolation buffer containing 1 mM EGTA, a residue of the EGTA was carried over with the mitochondria into the experimental buffer resulting in an estimated concentration of 40 μM EGTA.

All experiments were conducted at room temperature (25 °C) by using a precise experimental protocol shown in Fig. 1. At t=− 90 s, mitochondria were added to the experimental buffer resulting in a final mitochondrial protein concentration of 0.5 mg/ml for all samples. At t=0 s, pyruvic acid (PA, 0.5 mM), which was adjusted to pH 7.15, was added. At t=120 s, the mitochondrial suspension was exposed to 10, 20, 30 or 40 μM $CaCl_2$ to activate the CU. At t=300 s, ruthenium red (RR, 25 μM) was given to block the CU and to prevent further Ca^{2+} uptake or re-uptake. At t= 360 s, mitochondrial suspension was exposed to 0, 1, 2.5, 5, 10 or 20 mM NaCl to induce Na^+/Ca^{2+} exchange via the NCE. The experimental buffer, PA and all other reagents, except for the added NaCl, were Na^+-free to prevent NCE activation before adding NaCl. To avoid differences in buffer volume, the vehicle (deionized H_2O) was used for 0 μM $CaCl_2$ and 0 mM NaCl. To verify that the observed Na^+-induced Ca^{2+} exchange was actually achieved via the NCE, additional experiments were conducted in the presence of the NCE-inhibitor CGP-37157 (25 μM; Tocris Bioscience, Minneapolis, MN), which was dissolved in DMSO. All chemicals were obtained from Sigma-Aldrich (St. Louis, MO) unless noted otherwise.

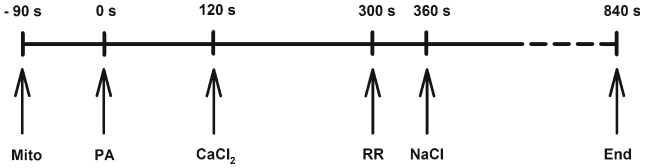

Fig. 1 Protocol and timeline. At t=− 90 s mitochondria (Mito, 0.5 mg) were added to the Na^+-free buffer solution (1 ml). Substrate, pyruvic acid (PA, 0.5 mM), was added at t=0 s to energize mitochondria (state 2) followed by either 0, 10, 20, 30 or 40 μM $CaCl_2$ at t=120 s. Ruthenium red (RR, 25 μM) was added at t=300 s to block further Ca^{2+} uptake into the matrix via the Ca^{2+} uniporter (CU). At t=360 s mitochondrial suspension was exposed to either 0, 1, 2.5, 5, 10 or 20 mM NaCl to activate the Na^+/Ca^{2+} exchanger (NCE). Experiments measuring extra-matrix and matrix free $[Ca^{2+}]$, NADH or pH_m were stopped at t=840 s. In experiments measuring $\Delta\Psi_m$ or matrix volume, CCCP (4 μM) or valinomycin (10 nM) was added at t=900 s, respectively, and experiments were stopped at t=1,020 s

Fluorescence measurements

Fluorescence spectrophotometry (Qm-8, Photon Technology International, Birmingham, NJ) was used to determine $[Ca^{2+}]_e$ and $[Ca^{2+}]_m$, NADH, $\Delta\Psi_m$, pH_m, and matrix volume (Haumann et al. 2010). To measure $[Ca^{2+}]_m$ and pH_m, mitochondria were incubated with their respective fluorescence probes, dissolved in DMSO. These dyes have an acetoxymethyl group (AM) and require an incubation period of 20 min at room temperature (25 °C) to accumulate in the matrix. Once in the matrix, the AM is cleaved by esterases, and the dye is retained. To remove the remaining dye in the extra-matrix space another spin was conducted. Unlike $[Ca^{2+}]_m$ and pH_m, measurements of $[Ca^{2+}]_e$, $\Delta\Psi_m$, NADH and matrix volume do not require incubation with a dye during the isolation procedure. But to ensure identical conditions in all experiments, these mitochondria were incubated for 20 min at 25 °C with the appropriate concentration of DMSO used for indo-1 AM and BCECF AM.

To minimize errors and to avoid interference between different fluorescence dyes, isolated mitochondria were always incubated with either indo-1 AM, BCECF AM, or the vehicle (DMSO). $[Ca^{2+}]_e$ and $\Delta\Psi_m$ were measured by directly adding the appropriate dye to the experimental buffer.

Measurements of NADH and matrix volume did not require addition of a fluorescent probe and were conducted solely in vehicle-incubated (DMSO) mitochondria. Viability of mitochondria (0.5 mg/ml) was verified by measuring respiration at the beginning and at the end of fluorescence measurements using a Clark type O_2 electrode (MT200A, Strathkelvin Instruments, Glasgow, UK). Respiratory control indices (RCIs) were obtained by calculating the ratio of state 3 respiration to state 4 respiration with 0.5 mM pyruvic acid (PA) and 250 μM ADP. The mean RCIs (± SEM) were 12.08 (± 1.55) at the beginning of the fluorescence experiments and 8.51 (± 0.48) after 6 h. These RCI values verified functional coupling of the isolated mitochondria and their relative stability during the duration of the experiments.

Measurement of matrix free $[Ca^{2+}]$

$[Ca^{2+}]_m$ was measured by incubating the mitochondria with the emission-ratiometric dye indo-1 AM (5 μM). Indo-1 (Invitrogen™, Eugene, OR) is a fluorescent probe that binds to Ca^{2+} with a vendor-given dissociation constant (K_d) of approximately 220 nM. However, in this and other recent studies by our group, we determined a K_d of 330 nM (Agarwal et al. 2012) that more accurately reflects our experimental conditions. The emission wavelength (λ_{em}) of indo-1 shifts from 456 nm to 390 nm on binding to Ca^{2+} at an excitation wavelength (λ_{ex}) of 350 nm. The ratio of the two emission wavelengths corrects for differences in the amount of dye taken up into mitochondria. Since emission and excitation signals at these wavelengths are influenced by NADH autofluorescence, background emission signals at 390 and 456 nm were separately obtained and subtracted from the corresponding emission signals for indo-1 before calculating the ratios (R). For calibration, it was necessary to obtain ratios when all indo-1 had become bound to Ca^{2+} (R_{max}) and when no Ca^{2+} was bound to indo-1 (R_{min}). To determine these ratios, experiments were conducted in PA energized mitochondria using 500 nM cyclosporine A, 500 μM $CaCl_2$ for R_{max}, and A23187 (Ca^{2+}-ionophore) in the presence of 2.5 mM EGTA for R_{min}. The $[Ca^{2+}]_m$ was calculated using the following equation (Eq. 6) (Grynkiewicz et al. 1985):

$$\left[Ca^{2+}\right]_m = K_d \cdot \frac{S_{f2}}{S_{b2}} \cdot \frac{R - R_{min}}{R_{max} - R} \quad (1)$$

K_d is 330 nM, S_{f2} is the signal intensity of free indo-1 measured at 456 nm and S_{b2} is the signal intensity of Ca^{2+}-saturated indo-1 measured at 456 nm. Their values were obtained from the R_{max} and R_{min} experiments, which were done for each preparation. The individual $[Ca^{2+}]_m$ were scaled to the averaged $[Ca^{2+}]_m$ of each group at t=330 s (for protocol and timeline see above) to monitor the dynamics of the NCE. It is important to emphasize that the measured $[Ca^{2+}]_m$ reflects only the concentration of free Ca^{2+} and not the total Ca^{2+} content (i.e. bound and unbound).

Measurement of extra-matrix free $[Ca^{2+}]$

$[Ca^{2+}]_e$ was measured using indo-1 pentapotassium salt (PP) when added to the experimental buffer (1 μM). This form of indo-1 is not able to permeate the matrix. Calibration in the presence of mitochondria was slightly different from the one used for indo-1 AM. R_{min} was measured in experimental buffer containing 2.5 mM EGTA, while R_{max} was determined in the experimental buffer containing 40 μM EGTA and 10 mM $CaCl_2$. Measurement and calculation of $[Ca^{2+}]_e$ were conducted in the same manner as for $[Ca^{2+}]_m$ (see above).

Measurement of NADH

NADH autofluorescence signals measured at λ_{ex} of 350 nm and λ_{em} of 456 nm were used to correct for the background changes while measuring indo-1 fluorescence. To ensure identical levels of endogenous NADH, mitochondria used for NADH and indo-1 experiments were obtained from the same preparation of isolated mitochondria. Furthermore, NADH autofluorescence signals were used separately to validate Ca^{2+}-dependent effects on mitochondrial NADH levels. For calibration, the NADH pool was either fully oxidized (0 %) with the respiratory uncoupler carbonyl cyanide m-chlorophenyl hydrazone (CCCP, 4 μM), or fully reduced (100 %) with the complex-I-blocker rotenone (10 μM). NADH values were scaled for each group to their average at t=100 s (for protocol and timeline see above). Any significant effects on NADH by $CaCl_2$ and NaCl were determined at t=840 s and statistically compared among the groups.

Measurement of membrane potential

Mitochondrial membrane potential ($\Delta\Psi_m$) was measured using the lipophilic dye TMRM (Invitrogen™, Eugene, OR) in a ratiometric excitation approach (Scaduto and Grotyohann 1999). TMRM (1 μM), dissolved in DMSO, was separately added to the experimental buffer. Fluorescence changes were detected by two λ_{ex} (546 and 573 nm) and one λ_{em} (590 nm). By using this ratiometric approach the entire method is less susceptible to variations in dye concentration and fluorometer excitation energy (Scaduto and Grotyohann 1999). Mitochondrial uptake and release of TMRM depend on $\Delta\Psi_m$ and are accompanied by changes in the excitation spectrum. In the presence of TMRM, hyperpolarization induces a decrease in fluorescence intensity at 546 nm and an increase at 573 nm. On the contrary, a depolarization

causes a decrease in fluorescence intensity at 573 nm and an increase at 546 nm. The calculated ratio of both excitation wavelengths (573/546) is proportional to $\Delta\Psi_m$ and has the advantage of a broader dynamic range when compared to a single wavelength technique (Scaduto and Grotyohann 1999). Measured ratios were scaled for each group to their average photon counts at t=100 s (for protocol and timeline see above). Unlike the NADH measurements, $\Delta\Psi_m$ was measured at 0, 20 or 40 μM $CaCl_2$ combined with 0, 5 or 20 mM NaCl resulting in nine experimental groups. Any significant effects on $\Delta\Psi_m$ by adding $CaCl_2$ and NaCl were assessed at t=840 s (for protocol and timeline see above) and statistically compared among the groups. At the end of the protocol at t=900 s, CCCP (4 μM) was added to induce a maximal depolarization.

Measurement of matrix pH

Matrix pH (pH_m) was measured using BCECF AM (5 μM, Invitrogen™, Eugene, OR), which is a probe that fluoresces more in an alkaline medium and less in an acidic medium. Therefore, an increase in signal intensity at λ_{ex} of 504 nm and λ_{em} of 530 nm indicates matrix alkalinization. The measured signals were scaled for each group to their average photon counts at t=100 s (for protocol and timeline see above). Detected fluorescence was converted to pH units by measuring the BCECF signal from tritonized (1 % triton X-100) mitochondria in experimental buffers with known pH values (7.00, 7.15, 7.30, 7.45 and 7.60). A linear slope was obtained from this calibration technique, which enabled the calculation of the pH_m by its signal fluorescence intensity. As described for the $\Delta\Psi_m$ measurements above, the same combinations of different amounts of $CaCl_2$ and NaCl were used and significant effects were assessed in the same manner.

Measurement of matrix volume

Matrix volume was determined by the light scattering technique at λ_{ex} of 520 nm and λ_{em} of 520 nm (Aldakkak et al. 2010). Measured signals were scaled for each group to their average photon counts at t=100 s (for protocol and timeline see above). As described for the $\Delta\Psi_m$ measurements, the same combinations of $CaCl_2$ and NaCl were used and significant effects were assessed in the same manner. To confirm mitochondrial swelling, at the end of the protocol (t=900 s) maximal volume expansion was induced by adding valinomycin (10 nM), a K^+-specific ionophore.

Statistical analyses

Data were transferred from PTI FelixGX (Version 3) into Microsoft® Excel® (2007). IBM® SPSS® (Version 19) was used to execute statistical analysis, which was performed using one-way analysis of variance followed by post hoc Student-Newman-Keuls' test. Changes were considered statistically significant when the p-value was < 0.05. Data for analyses were collected at the times noted above and are presented as mean ± SEM.

Results

Changes in extra-matrix free $[Ca^{2+}]$

We monitored Ca^{2+} uptake and release in isolated mitochondria (0.5 mg/ml) by using a defined protocol (Fig. 1) with multiple combinations of different $CaCl_2$ and NaCl boluses, while measuring $[Ca^{2+}]_e$ (Fig. 2a, b, c, d and e). To summarize the Ca^{2+} uptake dynamics obtained by adding different amounts of $CaCl_2$, corresponding $[Ca^{2+}]_e$ at specified times (60, 120 and 300 s) were averaged and are presented in Fig. 2f as a function of $[CaCl_2]$ (0, 10, 20, 30 or 40 μM). Baseline $[Ca^{2+}]_e$, determined after adding PA at t=60 s (Fig. 2f, blue line), were not different among all $CaCl_2$ groups (~ 110 nM). In the presence of 40 μM EGTA, adding different amounts of $CaCl_2$ at t=120 s (Fig. 2f, red line) induced a rapid, concentration-dependent rise in $[Ca^{2+}]_e$ (~ 110, 350, 850, 1,550, 2,200 nM). After reaching a peak, $[Ca^{2+}]_e$ decreased as a result of Ca^{2+} uptake via the CU. This Ca^{2+} uptake was blocked by ruthenium red (RR) in a separate set of experiments (data not shown). The observed decrease in $[Ca^{2+}]_e$ was faster in the 30 and 40 μM $CaCl_2$ groups (Fig. 2d and e) than in to the 10 and 20 μM $CaCl_2$ groups (Fig. 2b and c). Subsequent addition of RR at t=300 s (Fig. 2f, green line) prevented any further Ca^{2+} uptake resulting in various levels of $[Ca^{2+}]_e$ (~ 110, 300, 450, 450, 470 nM). Administration of NaCl (0, 1, 2.5, 5, 10 or 20 mM) at t=360 s led to a concentration-dependent increase in $[Ca^{2+}]_e$, indicating an effective Na^+-induced Ca^{2+} extrusion (Fig. 2a, b, c, d and e). This increase in $[Ca^{2+}]_e$ caused by adding various amounts of NaCl at different $[CaCl_2]$ resulted in multiple patterns of Ca^{2+} dynamics (Fig. 2a, b, c, d and e). The change of the patterns proceeded in an orderly fashion with increasing $[CaCl_2]$ (Fig. 2a, b, c, d and e), whereby these patterns became more distinct at higher $[CaCl_2]$ (Fig. 2c, d and e) compared to lower $[CaCl_2]$ (Fig. 2a and b). The amount of mitochondrial Ca^{2+} extruded in exchange for extra-matrix Na^+ was dependent on the added NaCl as well as on the available $[Ca^{2+}]_m$.

Changes in matrix free $[Ca^{2+}]$

$[Ca^{2+}]_m$ (Fig. 3a, b, c, d and e) was measured under identical conditions and protocol (Fig. 1) as for $[Ca^{2+}]_e$ experiments. To summarize the Ca^{2+} uptake dynamics obtained by adding different $CaCl_2$ amounts, corresponding $[Ca^{2+}]_m$ at specified times (60, 120 and 300 s) were averaged and are presented in

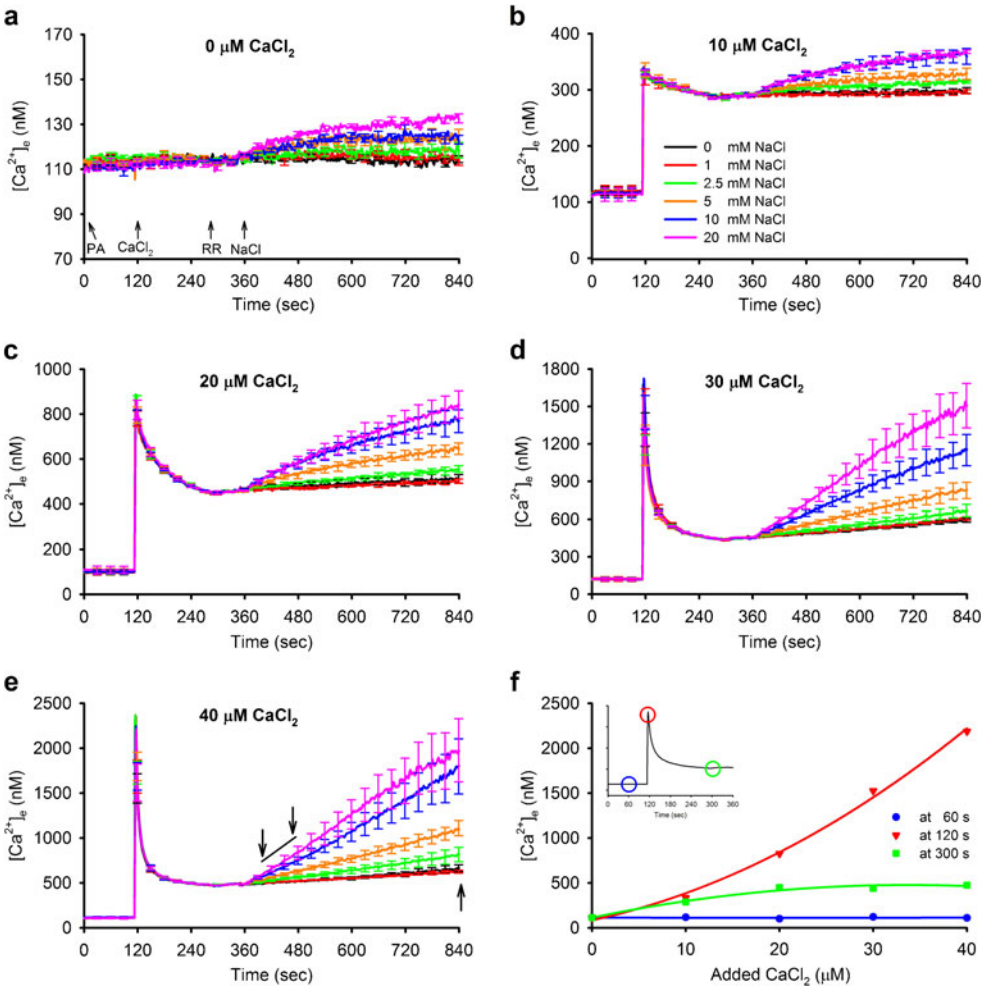

Fig. 2 Extra-matrix free $[Ca^{2+}]$. Panels **a**-**e** show how extra-matrix free $[Ca^{2+}]$ ($[Ca^{2+}]_e$) changed over time with addition of different amounts of NaCl (0–20 mM) at each $[CaCl_2]$ (0–40 μM). Note in Panels **b**-**e** that after a rapid rise in $[Ca^{2+}]_e$ and its decline as extra-matrix Ca^{2+} entered the matrix via the CU, added extra-matrix NaCl caused an increase in $[Ca^{2+}]_e$ via activation of the NCE. Additionally, Panel **e** indicates time intervals (*arrows*) used to derive the rate of change in $[Ca^{2+}]_e$ (= slope between 380 and 480 s) via the NCE and the final $[Ca^{2+}]_e$ at the end of each experiment (*single arrow*). The time course of Ca^{2+} uptake is summarized in Panel **f**, which illustrates $[Ca^{2+}]_e$ as a function of $[CaCl_2]$ at three specified time points (see inset, data are obtained from Panels **a**-**e**). Note in Panel **f** that best fitting trendlines are placed through all $[Ca^{2+}]_e$ of the same time points (60, 120, 300 s). Data in Panels **a**-**e** were obtained from a mitochondrial protein concentration of 0.5 mg/ml and are presented as mean of 4 individual experiments ± SEM

Fig. 2f as a function of $[CaCl_2]$ (0, 10, 20, 30 or 40 μM). Baseline $[Ca^{2+}]_m$, after adding PA at t=60 s (Fig. 3f, blue line), were not different among all $CaCl_2$ groups (~ 240 nM). In Fig. 3a, the 0 μM $CaCl_2$ group showed a slow gradual increase in $[Ca^{2+}]_m$, which could be attributed to a small amount of Ca^{2+} present in the experimental buffer despite the presence of 40 μM EGTA. To confirm this, additional experiments revealed that this slight increase in $[Ca^{2+}]_m$ was nullified when 1 mM EGTA or RR was present in the buffer (data not shown).

Adding $CaCl_2$ induced a rapid, concentration-dependent increase in $[Ca^{2+}]_m$ (~ 260, 360, 800, 1,200, 1,700 nM) at t=120 s (Fig. 3f, red line). At 20, 30 and 40 μM $CaCl_2$, $[Ca^{2+}]_m$ quickly approached a concentration-dependent level (Fig. 3c, d and e), whereas at 0 and 10 μM $CaCl_2$ Ca^{2+} uptake proceeded more slowly (Fig. 3a and b). At t=300 s (Fig. 3f, green line) levels of $[Ca^{2+}]_m$ were different among all $CaCl_2$ groups (~ 330, 600, 1,200, 1,350, 1,600 nM). Adding NaCl at t=360 s induced Na^+/Ca^{2+} exchange and caused a concentration-dependent decrease in $[Ca^{2+}]_m$. The NCE inhibitor CGP-37157 blocked Na^+/Ca^{2+}-exchange in the presence of 20 mM NaCl (data not shown), which was consistent with no addition of NaCl (0 mM); this indicates that the observed Na^+-induced Ca^{2+} exchange was mediated solely by the NCE.

The amount of Ca^{2+} extruded in exchange for extra-matrix Na^+ monitored by changes in $[Ca^{2+}]_m$ was dependent on the added NaCl and on the available $[Ca^{2+}]_m$. However, the patterns of Ca^{2+} dynamics obtained from $[Ca^{2+}]_m$ measurements (Fig. 3a, b, c, d and e) became less distinct at higher $[CaCl_2]$ (Fig. 3d and e) compared to lower $[CaCl_2]$ (Fig. 3a and b) and thus substantially deviated from those obtained from $[Ca^{2+}]_e$ measurements (Fig. 2a, b, c, d and e).

Quantifying Na^+/Ca^{2+} exchange derived from the rates of change in $[Ca^{2+}]_e$ and $[Ca^{2+}]_m$

The effects of adding $CaCl_2$ and NaCl on $[Ca^{2+}]_e$ and $[Ca^{2+}]_m$ at the end of each experiment, as indicated in Figs. 2e and 3e (t=840 s), are summarized in Fig. 4a, b and c. These averaged $[Ca^{2+}]_e$ and $[Ca^{2+}]_m$ were separately obtained from Figs. 2a, b, c, d and e and 3a, b, c, d and e and are shown as a function of

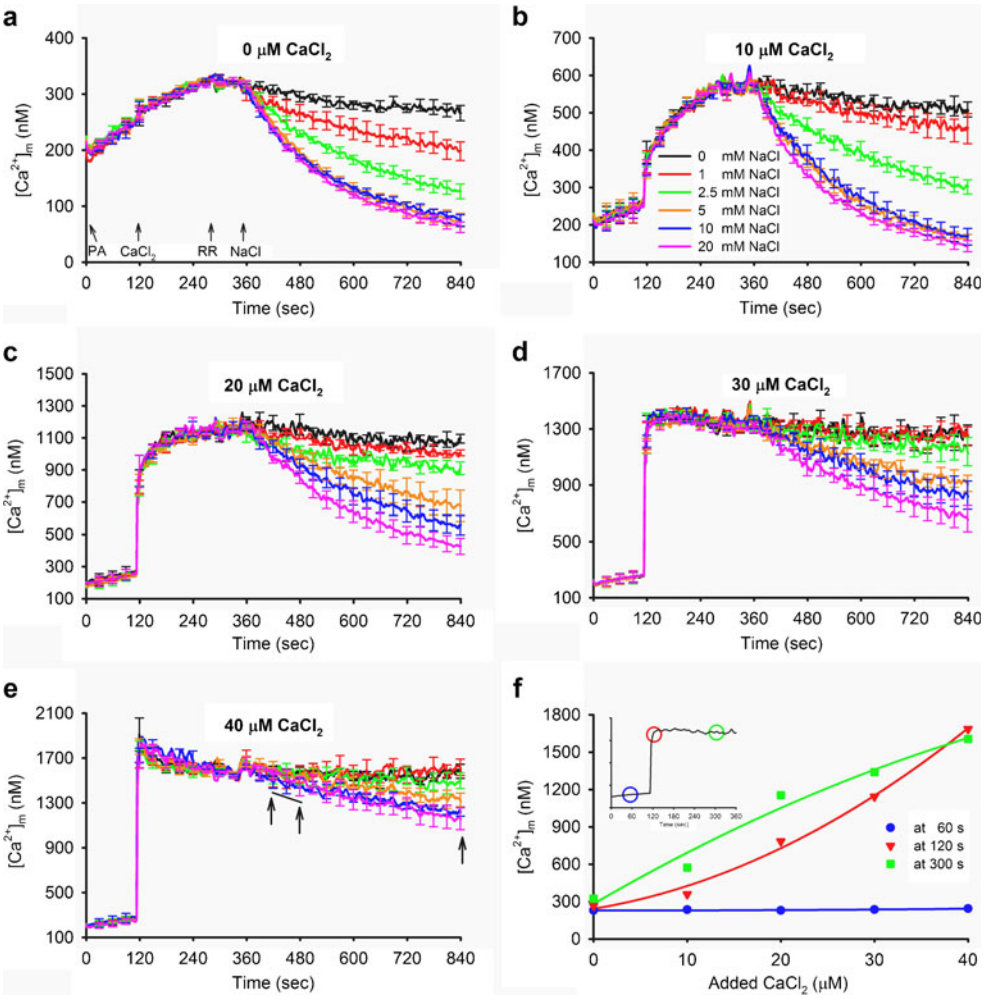

Fig. 3 Matrix free $[Ca^{2+}]$. Panels **a-e** show how matrix free $[Ca^{2+}]$ ($[Ca^{2+}]_m$) changed over time with addition of different amounts of NaCl (0–20 mM) at each $[CaCl_2]$ (0–40 μM). Note that after a rapid rise in $[Ca^{2+}]_m$ as extra-matrix Ca^{2+} entered the matrix via the CU (Panels **b-e**), extra-matrix Na^+ caused $[Ca^{2+}]_m$ to decrease via activation of the NCE. Additionally, Panel **e** indicates time intervals (*arrows*) used to derive the rate of change in $[Ca^{2+}]_m$ (= slope between 380 and 480 s) via the NCE and the final $[Ca^{2+}]_m$ at the end of each experiment (*single arrow*). The time course of Ca^{2+} uptake is summarized in Panel **f**, which illustrates $[Ca^{2+}]_m$ as a function of $[CaCl_2]$ at three specified time points, 60, 120 and 300 s (see inset, data are obtained from Panels **a-e**). Data in Panels **a-e** were obtained from a mitochondrial protein concentration of 0.5 mg/ml and are presented as mean of 4 individual experiments ± SEM

[NaCl] (Fig. 4a and b) and are also plotted against each other (Fig. 4c). For a given $[CaCl_2]$ of 20, 30 or 40 μM, $[Ca^{2+}]_e$ increased by adding NaCl (Fig. 4a). This effect was less at 0 and 10 μM $CaCl_2$ than at higher $[CaCl_2]$. For any given $[CaCl_2]$, $[Ca^{2+}]_m$ decreased considerably in the presence of 1–5 mM NaCl (Fig. 4b), whereas 10 or 20 mM NaCl had almost no additional effect on $[Ca^{2+}]_m$. The correlation between $[Ca^{2+}]_e$ and $[Ca^{2+}]_m$ with respect to added $CaCl_2$ is illustrated in Fig. 4c. Each $CaCl_2$ group consists of data from six [NaCl] and was best fitted with linear trendlines, which shifted up and to the right by increasing $[CaCl_2]$.

Na^+-induced Ca^{2+} exchange via the NCE was quantified by determining the rates of change in $[Ca^{2+}]_e$ and $[Ca^{2+}]_m$. Thus, the slope over the time interval 380–480 s was separately derived for each combination of various $[CaCl_2]$ and [NaCl], as indicated in Figs. 2e and 3e. To better appreciate the dynamics of NCE, the rates of change in $[Ca^{2+}]_e$ and $[Ca^{2+}]_m$ were plotted against added NaCl (Fig. 5a and b). On the one hand, the rate of change in $[Ca^{2+}]_e$ (Fig. 5a) rose in a concentration-dependent manner for different amounts of NaCl at a defined $[CaCl_2]$. On the other hand, the rate of change in $[Ca^{2+}]_e$ increased in a concentration-dependent manner for a defined [NaCl] after adding different amounts of $CaCl_2$ (Fig. 5a). The maximal rate of change in $[Ca^{2+}]_e$ was reached at 40 μM $CaCl_2$ and 20 mM NaCl (Fig. 5a). These findings for $[Ca^{2+}]_e$ were supported only in part by the rates of change in $[Ca^{2+}]_m$ (Fig. 5b). The rate of change in $[Ca^{2+}]_m$ increased in an almost concentration-dependent manner by adding increasing amounts of NaCl at a given $[CaCl_2]$. However, by increasing [NaCl] (e.g. 5, 10 or 20 mM) at a $[CaCl_2]$ of 30 μM and higher the rate of change in $[Ca^{2+}]_m$ decreased compared to the same [NaCl] at a $[CaCl_2]$ of 20 μM. The maximal rate of change in $[Ca^{2+}]_m$ was reached at 20 μM $CaCl_2$ with 20 mM NaCl (Fig. 5b).

To visually demonstrate these apparent dissimilarities, we plotted the corresponding rates of change in $[Ca^{2+}]_e$ and $[Ca^{2+}]_m$ against each other (Fig. 5c). Each $CaCl_2$ group contains data from six different [NaCl] that were best fitted by linear trendlines. The slopes of the trendlines shifted to the right as $[CaCl_2]$ increased, which demonstrates that the rates of change in $[Ca^{2+}]_e$ and $[Ca^{2+}]_m$ behaved differently at a given $[CaCl_2]$ when challenged with different extra-matrix [NaCl]. At a given $[CaCl_2]$ (0, 10 or 20 μM), the rates of change in $[Ca^{2+}]_m$ were higher for any [NaCl] than the rates

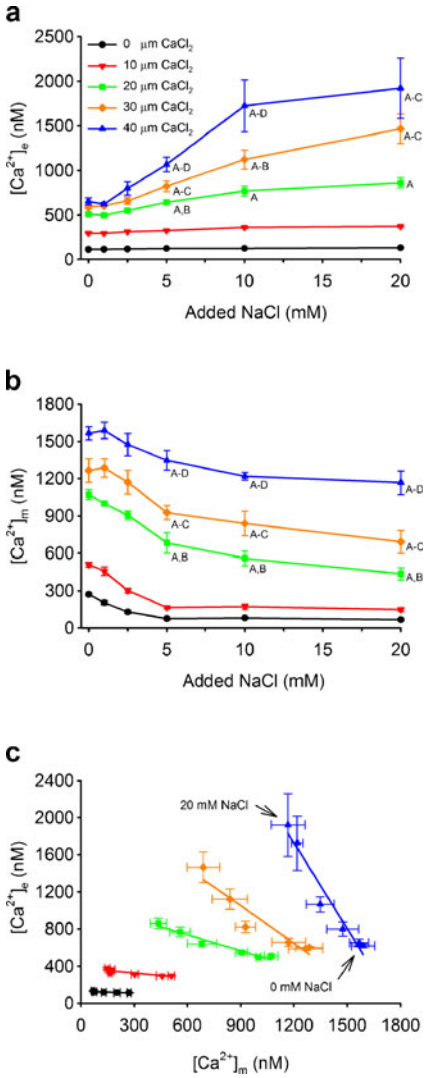

Fig. 4 Final extra-matrix free $[Ca^{2+}]$ and matrix free $[Ca^{2+}]$. Panels **a** and **b** show the extra-matrix free $[Ca^{2+}]$ ($[Ca^{2+}]_e$) and matrix free $[Ca^{2+}]$ ($[Ca^{2+}]_m$) measured at the end of each experiment (see Figs. 2 and 3) as a function of [NaCl]. Panel **c** shows the correlation between $[Ca^{2+}]_e$ and $[Ca^{2+}]_m$ with respect to added $CaCl_2$. Each $CaCl_2$ group consists of data from each of the six [NaCl] (as indicated by the *arrows*), which were best fitted with linear trendlines. Data were obtained from a mitochondrial protein concentration of 0.5 mg/ml and are presented as mean ± SEM for both x and y-axes, where applicable. Significant differences ($p<0.05$) in $[Ca^{2+}]_e$ or $[Ca^{2+}]_m$ for a given NaCl (5, 10 and 20 mM): 'A' vs. 0 μM $CaCl_2$; 'B' vs. 10 μM $CaCl_2$; 'C' vs. 20 μM $CaCl_2$; 'D' vs. 30 μM $CaCl_2$

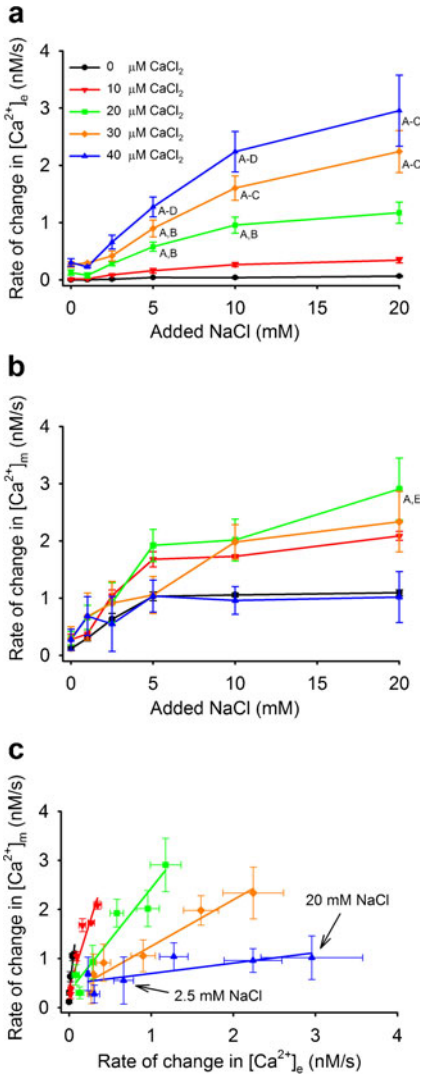

Fig. 5 Rates of change in matrix free $[Ca^{2+}]$ and extra-matrix free $[Ca^{2+}]$. Rates of change in extra-matrix free $[Ca^{2+}]$ ($[Ca^{2+}]_e$) and matrix free $[Ca^{2+}]$ ($[Ca^{2+}]_m$) were derived separately by determining the slope over a defined time interval (as indicated in Figs. 2e and 3e) for all experiments. Panels **a** and **b** show the rates of change in $[Ca^{2+}]_e$ and $[Ca^{2+}]_m$ as a function of [NaCl]. In Panel **c** corresponding rates of change in $[Ca^{2+}]_m$ and $[Ca^{2+}]_e$ are plotted against each other. Within each $CaCl_2$ group are the data from each of the six [NaCl] (as indicated by the *arrows*). Individual $CaCl_2$ group data were best fitted by linear trendlines. Data were obtained from a mitochondrial protein concentration of 0.5 mg/ml and are presented as mean ± SEM for both x and y-axes, where applicable. Significant differences ($p<0.05$) in $[Ca^{2+}]_e$ or $[Ca^{2+}]_m$ for a given NaCl (5, 10 and 20 mM): 'A' vs. 0 μM $CaCl_2$; 'B' vs. 10 μM $CaCl_2$; 'C' vs. 20 μM $CaCl_2$; 'D' vs. 30 μM $CaCl_2$; 'E' vs. 40 μM $CaCl_2$

of change in $[Ca^{2+}]_e$ under similar conditions. At 40 μM $CaCl_2$ and [NaCl] higher than 2.5 mM, rates of change in $[Ca^{2+}]_m$ were lower than the corresponding rates of change in $[Ca^{2+}]_e$. However, a direct comparison of data derived from the individual $[Ca^{2+}]_e$ and $[Ca^{2+}]_m$ measurements (Figs. 4a, b and c and 5a, b and c) is affected not only by differences in Ca^{2+} buffering properties between the two compartments, but also by the much larger extra-matrix volume than the matrix volume.

Changes in NADH, membrane potential, matrix pH and matrix volume with added $CaCl_2$ and NaCl

To evaluate the impact of Ca^{2+} uptake and release on mitochondrial bioenergetics, NADH, $\Delta\Psi_m$, pH_m and matrix

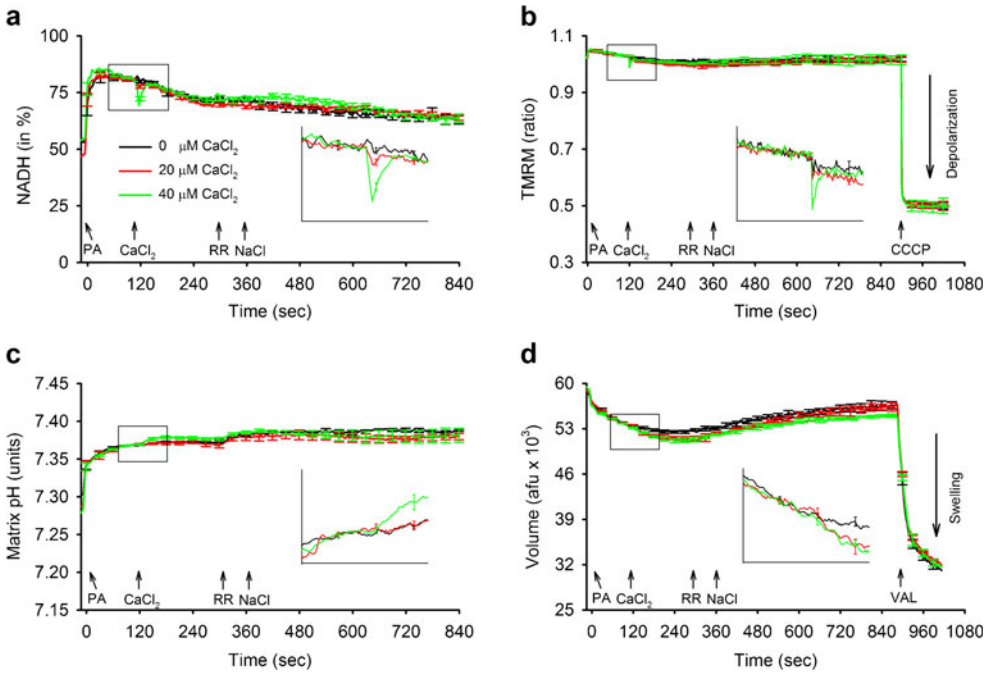

Fig. 6 NADH, membrane potential, matrix pH and matrix volume. Related experiments were conducted in tandem to monitor changes in NADH, membrane potential ($\Delta\Psi_m$), matrix pH (pH_m), and matrix volume using the same protocol depicted in Fig. 1. Panels **a**, **b**, **c** and **d** illustrate data for 0, 20 and 40 μM $CaCl_2$ combined with 5 mM NaCl as a function of time (see Supplement for other groups). Panel **a** shows changes in NADH expressed as a percentage. Note that adding $CaCl_2$ induced a transient concentration-dependent oxidation of NADH at t=120 s (see inset). Panel **b** shows changes in $\Delta\Psi_m$ monitored by TMRM fluorescence in a ratiometric excitation approach. At the end (t=900 s) of each experiment CCCP (4 μM) was added to induce maximal depolarization. Note that 40 μM $CaCl_2$ induced a transient depolarization of $\Delta\Psi_m$ at t=120 s (see inset). Panel **c** shows changes in pH_m monitored by BCECF fluorescence. Note that 40 μM $CaCl_2$ induced a slight increase in pH_m at t=120 s (see inset). Panel **d** shows changes in matrix volume measured by light scattering. At the end (t=900 s) of each experiment valinomycin (VAL, 10 nM), a K^+ ionophore, induced maximal matrix swelling. Note that 20 or 40 μM $CaCl_2$ induced a slight swelling (see inset). Data were obtained from a mitochondrial protein concentration of 0.5 mg/ml and are presented as mean of 3 individual experiments ± SEM

volume were measured using the same protocol and conditions as mentioned above for $[Ca^{2+}]_e$ and $[Ca^{2+}]_m$. Results for 5 mM NaCl at 0, 20 or 40 μM $CaCl_2$ are illustrated in Fig. 6, whereas data for 0 and 20 mM NaCl at the same $[CaCl_2]$ are shown in the Supplement (Figs. S1, S2, S3 and S4).

NADH (Fig. 6a) was assessed to provide the background autofluorescence measurements required to correct the indo-1 signals as well as to monitor changes in mitochondrial redox state. Addition of PA (t=0 s) induced an abrupt increase in NADH. The exposure of mitochondria to 30 (data not shown) or 40 μM $CaCl_2$ (t=120 s) caused a significant transient and reversible oxidation of NADH compared to 0 and 20 μM $CaCl_2$ (see inset Fig. 6a). Adding NaCl to activate the NCE did not significantly influence the level of NADH at t=840 s (see also Supplement Fig. S1).

The major driving force for Ca^{2+} uptake is $\Delta\Psi_m$ (Fig. 6b), which may be influenced by changes in the Ca^{2+} gradient via the CU and NCE. Like the change in NADH, 40 μM $CaCl_2$ induced a slight and transient membrane depolarization compared to 0 or 20 μM $CaCl_2$ (see inset Fig. 6b). Adding NaCl did not significantly alter the level of $\Delta\Psi_m$ at t=840 s. The maximal membrane depolarization induced by adding CCCP (t=900 s) was similar in magnitude for all groups (see also Supplement Fig. S2).

The pH gradient (Fig. 6c) influences not only the activity of the mitochondrial NHE or CHE, which in turn can influence the NCE, but also the Ca^{2+} buffering capacity. Like the change in NADH, adding PA to energize mitochondria caused an abrupt increase in pH_m (alkalinization) due to H^+ pumping. Exposure of mitochondria to 40 μM $CaCl_2$ induced a further increase in pH_m compared to 0 or 20 μM $CaCl_2$ (see inset Fig. 6c). Compared to 0 mM NaCl, pH_m was not altered in the presence of 5 or 20 mM NaCl (see also Supplement Fig. S3). The level of pH_m at t=840 s was nearly the same for all groups (~ 7.38).

Matrix volume (Fig. 6d) can be affected by changes in ionic gradients across the IMM. Adding PA induced a gradual volume increase due to mitochondrial energization. This volume expansion was slightly enhanced by 20 and 40 μM $CaCl_2$ compared to 0 μM $CaCl_2$ (see inset of Fig. 6d). The exposure of mitochondria to 5 or 20 mM NaCl at 0 and 20 μM $CaCl_2$ reduced matrix volume slightly

compared to 0 mM NaCl. In the presence of 0, 5 or 20 mM NaCl at 40 μM $CaCl_2$ matrix volume was not significantly altered compared to 0 and 20 μM $CaCl_2$ at t=840 s (see also Supplement Fig. S4). Adding valinomycin (t=900 s) induced a maximal matrix volume expansion that was similar in magnitude for all groups. However, the observed increase in matrix volume induced by 0, 5 or 20 mM NaCl at 0, 20 and 40 μM $CaCl_2$ was negligible compared to the maximal volume expansion caused by valinomycin.

Discussion

It is generally known that mitochondria are able to take up, buffer and release large amounts of Ca^{2+}, but it is not well understood how mitochondria do this under different Ca^{2+} loading conditions. Thus, the objective of our study was to investigate and characterize the dynamics of the mitochondrial Ca^{2+} uniporter (CU) and Na^+/Ca^{2+} exchanger (NCE) in regard to the Ca^{2+} buffering properties of the extra-matrix and matrix compartments under our experimental conditions. We postulated that Ca^{2+}- and Na^+-induced changes in $[Ca^{2+}]_e$ and $[Ca^{2+}]_m$ show dissimilar dynamics and that these dissimilarities are due to a strong and dynamic Ca^{2+} buffering of the matrix compartment. To test this, isolated mitochondria from guinea pig hearts were used to measure $[Ca^{2+}]_e$ and $[Ca^{2+}]_m$ (Figs. 2 and 3) following a defined protocol (Fig. 1) with multiple combinations of different [$CaCl_2$] and [NaCl]. Additional experiments were conducted to observe parallel effects on mitochondrial NADH, $\Delta\Psi_m$, pH_m and matrix volume.

Our results demonstrate first that addition of different amounts of $CaCl_2$ to the extra-matrix compartment induced a concentration-dependent increase in $[Ca^{2+}]_m$ (Fig. 3a, b, c, d and e). Subsequently adding NaCl at different [$CaCl_2$] caused different patterns of Ca^{2+} dynamics measured by changes in $[Ca^{2+}]_e$ and $[Ca^{2+}]_m$. Interestingly, these Ca^{2+} dynamics were not only dissimilar among different [$CaCl_2$] and [NaCl], but also between the extra-matrix and matrix compartments (Figs. 2a, b, c, d and e vs. 3a, b, c, d and e). To our knowledge, these salient observations of dynamic Ca^{2+} uptake and release have not been previously described in such a detailed and systematic manner. In addition, our data provided an opportunity to quantify the dynamic Ca^{2+} buffering system of the matrix compartment under our experimental conditions using a computational approach (see companion paper (Bazil et al. 2012)). Lastly, the observed activity of the CU in the presence of 40 μM $CaCl_2$ transiently influenced NADH, $\Delta\Psi_m$, pH_m and matrix volume (Fig. 6), whereas NCE activation did not substantially alter any of these variables.

Changes in $[Ca^{2+}]_e$ and $[Ca^{2+}]_m$ caused by Ca^{2+} uptake and release do not show reciprocal dynamics

Mitochondrial uptake of Ca^{2+} via the CU is dependent on the $\Delta\Psi_m$ and on the Ca^{2+} gradient across the IMM (Gunter and Sheu 2009; Pradhan et al. 2010b). In our study the uptake of different amounts of Ca^{2+} increased $[Ca^{2+}]_m$ in a concentration-dependent manner until RR was added (Fig. 3f), whereas the corresponding levels of $[Ca^{2+}]_e$ were very similar for 20, 30 or 40 μM $CaCl_2$ (Fig. 2f). Thus, the Ca^{2+} uptake patterns obtained from the measurements of $[Ca^{2+}]_e$ and $[Ca^{2+}]_m$ in the current study did not show reciprocal dynamics. This discrepancy is caused by a dynamic Ca^{2+} buffering of the matrix compartment that can be best observed from the Ca^{2+} uptake dynamics for 30 and 40 μM $CaCl_2$, as measured from the aspect of both the extra-matrix and matrix compartments (Figs. 2d and e vs. 3d and e). At these high [$CaCl_2$], the uptake of Ca^{2+} rapidly increased $[Ca^{2+}]_m$ to a certain level that was maintained until the addition of RR. Interestingly, the corresponding decrease in $[Ca^{2+}]_e$ lasted longer than the Ca^{2+} uptake observed by measuring $[Ca^{2+}]_m$ (Figs. 2d and e vs. 3d and e). This indicates that the extra-matrix Ca^{2+} taken up by mitochondria was immediately bound and so did not further increase $[Ca^{2+}]_m$.

In contrast to previous studies (Chalmers and Nicholls 2003; Wei et al. 2011), the NCE was not active under our experimental conditions until NaCl was added (t=360 s). This initial inactivity of the NCE was verified by additional experiments in the presence of CGP-37157. However, a possible extrusion of Ca^{2+} via the putative CHE cannot be ruled out in our experiments, since the CHE is known to exist in cardiac mitochondria (Gunter and Sheu 2009). This fact could explain why we observed a slight increase in $[Ca^{2+}]_e$ and decrease in $[Ca^{2+}]_m$ at 0 mM NaCl (Figs. 2a and 3a).

To quantify Ca^{2+} extrusion via the NCE at different [$CaCl_2$] and [NaCl], we first derived the rates of change in $[Ca^{2+}]_e$ and $[Ca^{2+}]_m$ over a specified time interval (Figs. 2e and 3e). The concentration-dependent relationship between the rate of change in $[Ca^{2+}]_e$ and added NaCl (Fig. 5a) was confirmed in part by the rate of change in $[Ca^{2+}]_m$ (Fig. 5b), while the concentration-dependent relationship between the rate of change in $[Ca^{2+}]_e$ and added $CaCl_2$ (Fig. 5a) deviated from the relationship derived by the rate of change in $[Ca^{2+}]_m$ (Fig. 5b). These differences in Ca^{2+} dynamics between the extra-matrix and matrix compartments can also be attributed to the different Ca^{2+} buffering properties of both compartments.

Since the extra-matrix Ca^{2+} is primarily buffered by EGTA, the obtained rates of change in $[Ca^{2+}]_e$ are likely to better represent the actual rate of Na^+-induced Ca^{2+} exchange. The concentration-dependent relationship shown in our study between the rates of change in $[Ca^{2+}]_e$ and added NaCl is consistent with an earlier study (Crompton

et al. 1976) on Na^+-induced Ca^{2+} efflux. That study demonstrated that the rate of Ca^{2+} efflux by adding NaCl (0–50 mM) proceeded in a sigmoid manner indicating a saturable NCE. A sigmoid relationship between Ca^{2+} efflux and added NaCl was also reported in another study (Kim and Matsuoka 2008) in permeabilized rat mycocytes, in which a sharp increase in Ca^{2+} efflux appeared within a narrow range of different [NaCl]. Although our study conditions were different, we observed a similar phenomenon when adding different amounts of NaCl at a defined [$CaCl_2$]. As shown in Fig. 5a for 20, 30 and 40 μM $CaCl_2$, the rate of change in $[Ca^{2+}]_e$ shows a sigmoid-like dependence on the added amount of NaCl with the greatest difference in the rate of change between 1 and 10 mM NaCl.

Our findings on an increase in the rate of change in $[Ca^{2+}]_e$ with added $CaCl_2$ and NaCl agree with a recent study by Wei et al. (Wei et al. 2011). In that study the authors reported a biphasic dependence of the rate of Ca^{2+} efflux on the added amount of NaCl because of a decrease in Ca^{2+} efflux by increasing [NaCl] in excess of 15 mM. In our study, adding NaCl increased the rate of change in $[Ca^{2+}]_e$ in a sigmoid manner (Fig. 5a), with a maximum at 20 mM NaCl. In contrast to the approach described in the Wei et al. study, in which NaCl was already present at the beginning of the experiments, we added NaCl to the Na^+-free mitochondrial suspension after blocking the CU to avoid an early activation of the NCE.

Mitochondrial Ca^{2+} buffering modulates Ca^{2+} dynamics

Although several experimental and computational studies on mitochondrial Ca^{2+} homeostasis have suggested the ability of mitochondria to buffer large amounts of Ca^{2+}, the precise mechanisms and functional principles of Ca^{2+} buffering, as well as its role in modulating Ca^{2+} dynamics, are not well understood. In part, this shortcoming arises from the lack of data on corresponding $[Ca^{2+}]_e$ and $[Ca^{2+}]_m$ measurements. Our data show unambiguously that $[Ca^{2+}]_e$ and $[Ca^{2+}]_m$ do not display reciprocal dynamics. The differences in Ca^{2+} buffering between the extra-matrix and matrix compartments may explain the observed differences in the Ca^{2+} dynamics.

The ability of mitochondria to buffer Ca^{2+} can be determined by calculating the Ca^{2+} buffering power (β) of both compartments. In our study, the buffering power of the extra-matrix compartment is predefined by a fixed composition of the experimental buffer, which contained 40 μM EGTA. On the other hand, the matrix Ca^{2+} buffering power is much more extensive and, with respect to our current observations, may change in a dynamic manner. This indicates that the matrix Ca^{2+} buffering power depends on the amount of Ca^{2+} taken up. This notion of dynamic matrix Ca^{2+} buffering is supported by our companion paper (Bazil et al. 2012), in which our experimental data on NCE dynamics were computationally analyzed to estimate the matrix Ca^{2+} buffering power ($\beta_{Ca,m}$) and to characterize the mitochondrial sequestration system. A basic prerequisite for quantification of the Ca^{2+} buffering power is the data on total and free $[Ca^{2+}]$ in the extra-matrix and matrix compartments. We measured changes in $[Ca^{2+}]_e$ and $[Ca^{2+}]_m$ during Ca^{2+} uptake and release, but not total $[Ca^{2+}]$, since such measurements are complex to undertake in a dynamic manner over the same time course. Thus, in our companion paper we developed and utilized a mathematical model based on the principle of mass conservation to determine the ratio of the rates of change of total and free matrix $[Ca^{2+}]$. Intriguingly, these computations confirm and substantiate our observations that the matrix Ca^{2+} buffering power is dynamically regulated depending on the amount of Ca^{2+} taken up into the matrix.

In general, matrix Ca^{2+} buffering capacity appears to be determined by several factors: those that define the maximal amount of retained Ca^{2+}, and those that define the threshold level for induction of Ca^{2+} release by opening of the mPTP (Chinopoulos and Adam-Vizi 2010). Both Ca^{2+} retention and release can be modulated by experimental conditions, for instance by changing the pH or the amount of phosphate or adenine nucleotides (Chinopoulos and Adam-Vizi 2010). Under our experimental conditions, adenine nucleotides did not play a role in matrix Ca^{2+} buffering, because they were not added to the experimental buffer. Small changes in pH_m were observed after adding large amounts of $CaCl_2$, but no significant changes in pH_m were detected by adding NaCl. It is widely believed that the major mechanism of Ca^{2+} storage in mitochondria is achieved by the formation of amorphous Ca^{2+}-phosphate precipitates (Chalmers and Nicholls 2003; Chinopoulos and Adam-Vizi 2010), which could be enhanced by various matrix proteins (e.g. annexins) serving as nucleation factors (Starkov 2010; Genge et al. 2007). The formation of Ca^{2+}-phosphate precipitates inside the matrix of isolated liver, brain and heart mitochondria has been reported previously (Chalmers and Nicholls 2003; Zoccarato and Nicholls 1982; Wei et al. 2012). Since phosphate (5 mM) was present in our experimental buffer from the beginning, the formation of Ca^{2+}-phosphate precipitates could conceivably explain in part the dynamic Ca^{2+} buffering power of the matrix compartment.

The formation and dissociation of Ca^{2+}-phosphate precipitates inside the matrix compartment are closely linked to pH_m, because the phosphate ion (PO_4^{3-}) concentration depends on the third power of the pH gradient (Nicholls and Chalmers 2004). Thus, formation of Ca^{2+}-phosphate precipitates requires alkaline conditions (pH>7.7) to take place at $[Ca^{2+}]_m$ below 2 μM (Nicholls and Chalmers 2004). However, at our $[Ca^{2+}]_m$ levels (< 2 μM) a pH in the range of 7.2–7.4 would not be conducive to formation of Ca^{2+}-phosphate precipitates in great quantities. We conclude that mechanisms other than the simple formation of Ca^{2+}-phosphate precipitates are likely to be involved in the matrix Ca^{2+} sequestration process.

Effects of Ca^{2+} uptake and release on NADH, membrane potential, matrix pH and matrix volume

Mitochondrial Ca^{2+} loading is believed to have a significant impact on mitochondrial function, especially respiration (Griffiths 2009; Camara et al. 2010). It has been reported that elevated $[Ca^{2+}]_m$ can increase NADH generation in part by stimulating Ca^{2+}-sensitive dehydrogenases of the TCA cycle (Griffiths 2009; Denton 2009). In our study the bioenergetic state was monitored by NADH measurements (Fig. 6a). Adding PA induced an abrupt increase in NADH due to an increase in TCA cycle activity, which is consistent with recent studies (Wei et al. 2011; Haumann et al. 2010; Agarwal et al. 2012). A significant rapid and transient drop in NADH (oxidation) was induced by 40 μM $CaCl_2$. This transient oxidation of NADH was associated with a similar transient decrease in $\Delta\Psi_m$ at the same time. Under physiologic conditions, mitochondrial NADH is consumed by the electron transport chain (ETC) to create a negative $\Delta\Psi_m$ across the IMM (−150 to −220 mV). The observed oxidation of NADH is consistent with an increase in ETC activity to restore $\Delta\Psi_m$.

The negative $\Delta\Psi_m$ is the primary driving force for Ca^{2+} uptake via the CU (Chinopoulos and Adam-Vizi 2010; Camara et al. 2011) and also part of the driving force for an electrogenic Na^+/Ca^{2+} exchange via the NCE (Jung et al. 1995; Kim and Matsuoka 2008). Hence, the transfer of net positive charges into the matrix during an electrogenic Na^+/Ca^{2+} exchange should be achieved at the expense of the $\Delta\Psi_m$ resulting in a partial depolarization. Indeed, we observed a transient mitochondrial membrane depolarization at 40 μM $CaCl_2$ that was associated with a transient oxidation of NADH (see insets Fig. 6a and b). The rapid transient decrease in $\Delta\Psi_m$ was likely restored by increased respiration, i.e. enhanced NADH oxidation and H^+ pumping.

The pH gradient across the IMM created by the ETC may be linked to the Ca^{2+} gradient via the CHE (directly) and NHE (indirectly). As noted above, we cannot exclude a slight contribution of the CHE to the Ca^{2+} extrusion because of a small increase in $[Ca^{2+}]_e$ and a corresponding decrease in $[Ca^{2+}]_m$ in the absence of NaCl. Previous studies in heart mitochondria demonstrated that the NHE effectively matches the Na^+ gradient to the H^+ gradient (Baysal et al. 1994; Jung et al. 1992; Crompton and Heid 1978). Furthermore, the NHE is thought to exchange ions much faster than the NCE indicating that the activity of the NHE determines the actual matrix concentration of Na^+ (Jung et al. 1992).

In our experiments, Ca^{2+} uptake via the CU and its release via the NCE occurred between pH_m 7.34 and 7.38 (Fig. 6c), which is in the pH_m range (7.2–7.6) reported by us and others (Santo-Domingo and Demaurex 2010; Haumann et al. 2010). Adding PA to the mitochondrial suspension induced an abrupt increase in pH_m (alkalinization) that was increased further by 40 μM $CaCl_2$. The slight increase in pH_m after adding $CaCl_2$ was probably due to enhanced activity of the TCA cycle to maintain the NADH level and a concomitant increase in H^+ pumping to re-establish the $\Delta\Psi_m$. Adding NaCl to the NCE did not significantly change pH_m in any $CaCl_2$ group. This is consistent with previous findings (Crompton et al. 1976), and so we therefore assume that the NHE maintains the Na^+ gradient across the IMM quite constant.

Matrix volume is essentially controlled by the osmotic balance between the extra-matrix and matrix compartments that is generated by the sum of cations, anions and other osmolytes across the IMM (Kaasik et al. 2007). Mitochondrial K^+ homeostasis plays an important role in volume regulation with a concerted interplay between K^+ uptake via the K^+ channels and K^+ efflux via the K^+/H^+ exchanger (Kaasik et al. 2007). Changes in matrix volume may regulate mitochondrial energy metabolism by affecting the efficiency of the TCA cycle enzymes and ETC (Camara et al. 2010). We observed that energizing mitochondria with PA induced an abrupt matrix volume expansion that was increased slightly more by 20 or 40 μM $CaCl_2$. The slight additional increase in matrix volume by adding $CaCl_2$ could be due to modulation of K^+ homeostasis by Ca^{2+}-dependent K^+-channel opening (Kaasik et al. 2007). Overall, compared to the maximal swelling induced by valinomycin, the observed changes in volume by different $[CaCl_2]$ and [NaCl] were negligible.

Mitochondrial NCE stoichiometry

There are several experimental and computational studies on the putative stoichiometry of the mitochondrial NCE (Pradhan et al. 2010a; Brand 1985; Baysal et al. 1994; Jung et al. 1995; Kim and Matsuoka 2008; Dash and Beard 2008; Affolter and Carafoli 1980). Most of them support an electrogenic exchange (Pradhan et al. 2010a; Baysal et al. 1994; Kim and Matsuoka 2008; Dash and Beard 2008). One of the earliest studies suggesting an electrogenic exchange for the NCE (Crompton et al. 1976) showed that the NCE kinetics exhibited saturation with high extra-matrix $[Na^+]$ resulting in a sigmoid curve. Based on this, it was suggested that more than one Na^+ was involved per cycle of exchange, as extrapolated from a Hill plot, to yield a $3Na^+$:$1Ca^{2+}$ stoichiometry (Crompton et al. 1976). However, other studies supported an electroneutral exchange for the NCE (Brand 1985; Affolter and Carafoli 1980; Li et al. 1992). For instance, Na^+/Ca^{2+} antiporters purified from beef heart mitochondria reconstituted into liposomes exchanged Ca^{2+} for Na^+ even in the presence of the uncoupler CCCP, which dissipates $\Delta\Psi_m$, indicating an electroneutral exchange (Li et al. 1992). To further complicate this discrepancy over the stoichiometry of the NCE, it was suggested that

the NCE might alternate between electroneutral and electrogenic exchange depending on the experimental conditions (Jung et al. 1995).

To determine the stoichiometry of the NCE in our study with multiple [$CaCl_2$] and [NaCl] combinations, we used a common approach that first assumes an electroneutral $2Na^+$:1 Ca^{2+} exchange (Baysal et al. 1994). Based on this assumption, the Ca^{2+} gradient across the IMM is equal to the square of the Na^+ gradient at equilibrium (Eq. 2). That is, Ca^{2+} would be exchanged for Na^+ until the energy contained in the electrochemical Ca^{2+} gradient is balanced by twice the energy of the electrochemical Na^+ gradient (Jung et al. 1995). The NHE equilibrates the Na^+ gradient to the H^+ gradient across the IMM (Eq. 3), but works much faster than the NCE in isolated mitochondria (Jung et al. 1995). By combining equations 2 and 3, equation 4 indicates that the Ca^{2+} gradient is equal to the square of the Na^+ or H^+ gradient at equilibrium (Baysal et al. 1994; Dash and Beard 2008):

$$\frac{[Ca^{2+}]_e}{[Ca^{2+}]_m} = \frac{[Na^+]_e^2}{[Na^+]_m^2} \tag{2}$$

$$\frac{[Na^+]_e}{[Na^+]_m} = \frac{[H^+]_e}{[H^+]_m} \tag{3}$$

$$\frac{[Ca^{2+}]_e}{[Ca^{2+}]_m} = \frac{[Na^+]_e^2}{[Na^+]_m^2} = \frac{[H^+]_e^2}{[H^+]_m^2} \tag{4}$$

Logically, under such conditions, a dissipation of the H^+ gradient would subsequently cause a collapse of the Na^+ and Ca^{2+} gradients. Under our experimental conditions, extra-matrix pH was maintained at 7.15 and pH_m was found to be around 7.38 (t=840 s) in all experimental groups (Fig. 6c, Supplement Fig. S3). Therefore, by inserting our data of $[Ca^{2+}]_m$ and $[Ca^{2+}]_e$, obtained from Fig 4a and b, along with $[H^+]_m = 10^{-7.38}$ and $[H^+]_e = 10^{-7.15}$ into equation 4, we determined that the Ca^{2+} gradients are notably greater than an electroneutral exchange would predict (see Table S1 in the Supplement). Based on this analysis, our study excludes the possibility of an electroneutral exchange via the NCE and suggests an electrogenic exchange.

Summary and conclusions

Our aim was to investigate and characterize the dynamics of mitochondrial Ca^{2+} uniporter (CU) and Na^+/Ca^{2+} exchanger (NCE) during Ca^{2+} uptake and release as well as parallel changes in NADH, $\Delta\Psi_m$, pH_m and matrix volume. The novelty of our study along with a major distinction from previous studies is that our approach demonstrates the impact of multiple combinations of different [$CaCl_2$] and [NaCl] on $[Ca^{2+}]_e$ and $[Ca^{2+}]_m$ in order to assess the influence of matrix Ca^{2+} buffering on Ca^{2+} dynamics.

Our results demonstrate that Ca^{2+} uptake and extrusion do not show reciprocal dynamics when viewed from the extra-matrix and matrix compartments. We observed a concentration-dependent relationship between added NaCl and the rate of change in $[Ca^{2+}]_e$. A concentration-dependent relationship observed between added $CaCl_2$ and the rates of change in $[Ca^{2+}]_e$ and $[Ca^{2+}]_m$ was not reciprocal. These differential responses can be attributed to the Ca^{2+} buffering power of the matrix, which changes dynamically based on the amount of Ca^{2+} taken up. In this way, mitochondria are able to take up and store a huge amount of Ca^{2+}, but they can also prevent an increase in $[Ca^{2+}]_m$ while maintaining cytosolic Ca^{2+} within a normal range. Furthermore, the Ca^{2+} dynamics were measured in tandem with mitochondrial NADH (redox state), $\Delta\Psi_m$, pH_m and matrix volume. All of these variables were affected by higher Ca^{2+} uptake (40 μM $CaCl_2$), but not by activation of the NCE. Lastly, by excluding an electroneutral Na^+/Ca^{2+} exchange via the NCE our data on Ca^{2+} dynamics indicate an electrogenic exchange.

Overall, our measurements of $[Ca^{2+}]_e$ and $[Ca^{2+}]_m$ furnish new insights into Ca^{2+} dynamics in regard to matrix Ca^{2+} buffering. These data were also utilized in our companion paper (Bazil et al. 2012), which computationally characterized the dynamics of Ca^{2+} uptake and release by the matrix Ca^{2+} sequestration system. More importantly, the computations from our companion paper support our experimental findings regarding the dynamic Ca^{2+} buffering power of the matrix compartment.

Acknowledgments The authors wish to thank Drs. A. Boelens, M. Aldakkak, B. Agarwal and K. Vinnakota for their valuable assistance. This work was supported by the National Institutes of Health grants R01-HL095122-02 (to AKSC and RKD) and R01-HL089514 (to DFS).

References

Affolter H, Carafoli E (1980) The Ca^{2+}-Na^+ antiporter of heart mitochondria operates electroneutrally. Biochem Biophys Res Commun 95(1):193–196

Agarwal B, Camara AK, Stowe DF, Bosnjak ZJ, Dash RK (2012) Enhanced charge-independent mitochondrial free Ca^{2+} and attenuated ADP-induced NADH oxidation by isoflurane: Implications for cardioprotection. Biochim Biophys Acta 1817(3):453–465

Aldakkak M, Stowe DF, Cheng Q, Kwok WM, Camara AK (2010) Mitochondrial matrix K^+ flux independent of large-conductance Ca^{2+}-activated K^+ channel opening. Am J Physiol Cell Physiol 298 (3):C530–C541

Baughman JM, Perocchi F, Girgis HS, Plovanich M, Belcher-Timme CA, Sancak Y et al (2011) Integrative genomics identifies MCU as an essential component of the mitochondrial calcium uniporter. Nature 476(7360):341–345

Baysal K, Jung DW, Gunter KK, Gunter TE, Brierley GP (1994) Na^+-dependent Ca^{2+} efflux mechanism of heart mitochondria is not a passive $Ca^{2+}/2Na^+$ exchanger. Am J Physiol 266(3 Pt 1):C800–C808

Bazil JN, Blomeyer CA, Pradhan RK, Camara AK, & Dash RK (2012) Modeling the calcium sequestration system in isolated guinea pig cardiac mitochondria. J Bioenerg Biomembr, accepted for publication

Bernardi P, Rasola A (2007) Calcium and cell death: the mitochondrial connection. Subcell Biochem 45:481–506

Bradford MM (1976) A rapid and sensitive method for the quantitation of microgram quantities of protein utilizing the principle of protein-dye binding. Anal Biochem 72:248–254

Brand MD (1985) The stoichiometry of the exchange catalysed by the mitochondrial calcium/sodium antiporter. Biochem J 229(1):161–166

Brookes PS, Yoon Y, Robotham JL, Anders MW, Sheu SS (2004) Calcium, ATP, and ROS: a mitochondrial love-hate triangle. Am J Physiol Cell Physiol 287(4):C817–C833

Camara AK, Lesnefsky EJ, Stowe DF (2010) Potential therapeutic benefits of strategies directed to mitochondria. Antioxid Redox Signal 13(3):279–347

Camara AK, Bienengraeber M, Stowe DF (2011) Mitochondrial approaches to protect against cardiac ischemia and reperfusion injury. Front Physiol 2:13

Chalmers S, Nicholls DG (2003) The relationship between free and total calcium concentrations in the matrix of liver and brain mitochondria. J Biol Chem 278(21):19062–19070

Chinopoulos C, Adam-Vizi V (2010) Mitochondrial Ca^{2+} sequestration and precipitation revisited. FEBS J 277(18):3637–3651

Cox DA, Matlib MA (1993) A role for the mitochondrial Na^+-Ca^{2+} exchanger in the regulation of oxidative phosphorylation in isolated heart mitochondria. J Biol Chem 268(2):938–947

Crompton M, Heid I (1978) The cycling of calcium, sodium, and protons across the inner membrane of cardiac mitochondria. Eur J Biochem 91(2):599–608

Crompton M, Capano M, Carafoli E (1976) The sodium-induced efflux of calcium from heart mitochondria. Eur J Biochem 69(2):453–462

Dash RK, Beard DA (2008) Analysis of cardiac mitochondrial Na^+-Ca^{2+} exchanger kinetics with a biophysical model of mitochondrial Ca^{2+} handling suggests a 3:1 stoichiometry. J Physiol 586 (13):3267–3285

Dash RK, Qi F, Beard DA (2009) A biophysically based mathematical model for the kinetics of mitochondrial calcium uniporter. Biophys J 96(4):1318–1332

De Stefani D, Raffaello A, Teardo E, Szabo I, Rizzuto R (2011) A forty-kilodalton protein of the inner membrane is the mitochondrial calcium uniporter. Nature 476(7360):336–340

Dedkova EN, Blatter LA (2008) Mitochondrial Ca^{2+} and the heart. Cell Calcium 44(1):77–91

Denton RM (2009) Regulation of mitochondrial dehydrogenases by calcium ions. Biochim Biophys Acta 1787(11):1309–1316

Genge BR, Wu LN, Wuthier RE (2007) In vitro modeling of matrix vesicle nucleation: synergistic stimulation of mineral formation by annexin A5 and phosphatidylserine. J Biol Chem 282(36):26035–26045

Graier WF, Frieden M, Malli R (2007) Mitochondria and Ca^{2+} signaling: old guests, new functions. Pflugers Arch 455(3):375–396

Griffiths EJ (2009) Mitochondrial calcium transport in the heart: physiological and pathological roles. J Mol Cell Cardiol 46(6):789–803

Grynkiewicz G, Poenie M, Tsien RY (1985) A new generation of Ca^{2+} indicators with greatly improved fluorescence properties. J Biol Chem 260(6):3440–3450

Gunter TE, Pfeiffer DR (1990) Mechanisms by which mitochondria transport calcium. Am J Physiol 258(5 Pt 1):C755–C786

Gunter TE, Sheu SS (2009) Characteristics and possible functions of mitochondrial Ca^{2+} transport mechanisms. Biochim Biophys Acta 1787(11):1291–1308

Halestrap AP (2009) Mitochondria and reperfusion injury of the heart - a holey death but not beyond salvation. J Bioenerg Biomembr 41 (2):113–121

Haumann J, Dash RK, Stowe DF, Boelens AD, Beard DA, Camara AK (2010) Mitochondrial free [Ca^{2+}] increases during ATP/ADP antiport and ADP phosphorylation: exploration of mechanisms. Biophys J 99(4):997–1006

Heinen A, Aldakkak M, Stowe DF, Rhodes SS, Riess ML, Varadarajan SG et al (2007) Reverse electron flow-induced ROS production is attenuated by activation of mitochondrial Ca^{2+}-sensitive K^+ channels. Am J Physiol Heart Circ Physiol 293(3):H1400–H1407

Hoppe UC (2010) Mitochondrial calcium channels. FEBS Lett 584 (10):1975–1981

Jung DW, Apel LM, Brierley GP (1992) Transmembrane gradients of free Na^+ in isolated heart mitochondria estimated using a fluorescent probe. Am J Physiol 262(4 Pt 1):C1047–C1055

Jung DW, Baysal K, Brierley GP (1995) The sodium-calcium antiport of heart mitochondria is not electroneutral. J Biol Chem 270(2):672–678

Kaasik A, Safiulina D, Zharkovsky A, Veksler V (2007) Regulation of mitochondrial matrix volume. Am J Physiol Cell Physiol 292(1): C157–C163

Kim B, Matsuoka S (2008) Cytoplasmic Na^+-dependent modulation of mitochondrial Ca^{2+} via electrogenic mitochondrial Na^+-Ca^{2+} exchange. J Physiol 586(6):1683–1697

Li W, Shariat-Madar Z, Powers M, Sun X, Lane RD, Garlid KD (1992) Reconstitution, identification, purification, and immunological characterization of the 110-kDa Na^+/Ca^{2+} antiporter from beef heart mitochondria. J Biol Chem 267(25):17983–17989

Nicholls DG, Chalmers S (2004) The integration of mitochondrial calcium transport and storage. J Bioenerg Biomembr 36(4):277–281

Olson ML, Chalmers S, McCarron JG (2012) Mitochondrial organization and Ca2+ uptake. Biochem Soc Trans 40(1):158–167

Palty R, Silverman WF, Hershfinkel M, Caporale T, Sensi SL, Parnis J et al (2010) NCLX is an essential component of mitochondrial Na^+/Ca^{2+} exchange. Proc Natl Acad Sci U S A 107(1):436–441

Paucek P, Jaburek M (2004) Kinetics and ion specificity of Na^+/Ca^{2+} exchange mediated by the reconstituted beef heart mitochondrial Na^+/Ca^{2+} antiporter. Biochim Biophys Acta 1659(1):83–91

Pradhan RK, Beard DA, Dash RK (2010a) A biophysically based mathematical model for the kinetics of mitochondrial Na^+-Ca^{2+} antiporter. Biophys J 98(2):218–230

Pradhan RK, Qi F, Beard DA, Dash RK (2010b) Characterization of membrane potential dependency of mitochondrial Ca^{2+} uptake by an improved biophysical model of mitochondrial Ca^{2+} uniporter. PLoS One 5(10):e13278

Santo-Domingo J, Demaurex N (2010) Calcium uptake mechanisms of mitochondria. Biochim Biophys Acta 1797(6–7):907–912

Saotome M, Katoh H, Satoh H, Nagasaka S, Yoshihara S, Terada H et al (2005) Mitochondrial membrane potential modulates regulation of mitochondrial Ca^{2+} in rat ventricular myocytes. Am J Physiol Heart Circ Physiol 288(4):H1820–H1828

Scaduto RC Jr, Grotyohann LW (1999) Measurement of mitochondrial membrane potential using fluorescent rhodamine derivatives. Biophys J 76(1 Pt 1):469–477

Starkov AA (2010) The molecular identity of the mitochondrial Ca^{2+} sequestration system. FEBS J 277(18):3652–3663

Wei AC, Liu T, Cortassa S, Winslow RL, O'Rourke B (2011) Mitochondrial Ca^{2+} influx and efflux rates in guinea pig cardiac mitochondria: low and high affinity effects of cyclosporine A. Biochim Biophys Acta 1813(7):1373–1381

Wei AC, Liu T, Winslow RL, O'Rourke B (2012) Dynamics of matrix-free Ca^{2+} in cardiac mitochondria: two components of Ca^{2+} uptake and role of phosphate buffering. J Gen Physiol 139(6):465–478

Zoccarato F, Nicholls D (1982) The role of phosphate in the regulation of the independent calcium-efflux pathway of liver mitochondria. Eur J Biochem 127(2):333–338